RSC Advances

ROYAL SOCIETY OF CHEMISTRY

www.rsc.org/advances

Electrochemical and Surface Characteristics of Sputter-Deposited Amorphous Mn-Zr-Cr Alloys in 1 M H_2SO_4 Solution

A.A. El-Moneim[1], M. Ezzat[1] and W. A. Badawy[2]*

[1]Materials Science and Engineering Department, Egypt–Japan University of Science and Technology, New Borg Al Arab, Alexandria, Egypt.
[2]Department of Chemistry, Faculty of Science, University of Cairo, Giza – Egypt

*Corresponding author: wbadawy@cu.edu.eg, wbadawy@sci.cu.edu.eg
Tel: 002 02 3567 6558, Fax: 002 02 35685799

Electrochemical and Surface Characteristics of Sputter-Deposited Amorphous Mn-Zr-Cr Alloys in 1 M H_2SO_4 Solution

A.A. El-Moneim[1], M. Ezzat[1] and W. A. Badawy[2]*

[1]Materials Science and Engineering Department, Egypt–Japan University of Science and Technology, New Borg Al Arab, Alexandria, Egypt.
[2]Department of Chemistry, Faculty of Science, University of Cairo, Giza – Egypt

ABSTRACT:

The effect of alloying zirconium and chromium on the electrochemical behavior of Mn-Zr-Cr alloys in H_2SO_4 solutions was investigated. The alloy surface was analyzed by XPS. The corrosion rates of the ternary Mn-Zr-Cr alloys are lower than those of the binary alloys containing the same amount of manganese and decrease with increasing the chromium content. The effect of alloying Cr and Zr with Mn is based on the synergistic interaction between their cations in the oxy-hydroxide passive films formed under open circuit conditions. The passivity enhancement is due to chromium enrichment in the surface film and the underlying alloy surface.

Keywords: Manganese alloys, Sputtered films, Polarization, XPS, Passive films.

*Corresponding author: wbadawy@cu.edu.eg, wbadawy@sci.cu.edu.eg
Tel: 002 02 3567 6558, Fax: 002 02 35685799

1. Introduction

The chemical and engineering applications of materials require the synergistic effects of various elements. For example, the corrosion resistance of many materials is often enhanced by coexisting alloying elements [1-8]. The prescribed amount of the alloying elements is required to enhance the corrosion resistance, and hence, the formation of a chemically homogeneous single phase. The formed single phase exceeds the solubility limits of the alloying elements at equilibrium, which is the most suitable way to get highly corrosion resistant materials. Sputtering technique is particularly an optimum method for the preparation of single phase solid solutions with the required characteristics even when the boiling point of a component is higher than the melting points of the others [1-13]. Current market and supply pressures on rare earth elements, components of technologically important advanced permanent magnets, are driving investigations into magnetic materials that can replace rare-earth-based alloys with more abundant and less strategically important elements. A promising strategy for realization of new concepts in permanent magnetic materials is to revisit the "classic" hard magnetic alloys that were widely used before the advent of the rare-earth-based super-magnets and, by employing advanced fabrication, such as sputter-deposition, and analysis methods, gain insight into the fundamentals governing their structure-magnetic property behavior for improved performance [14]. Among the list of materials targeted for this purpose is the ferromagnetic manganese (Mn)-based alloys.

The failure to produce corrosion-resistant manganese-based alloys is due to the very low solubility of passivating elements and valve metals in the metal. By utilizing the advantage of the sputtering technique, a series of homogeneous single phase binary manganese-valve metal alloys were prepared successfully. The electrochemical behavior of these sputter-deposited alloys was investigated extensively in neutral and alkaline media containing chloride ions; and all these

alloys exhibited superior corrosion resistance [12-19]. However, scarce information is available about their behavior in acidic media [17,18]. The effect of alloying chromium as passivating element on the behavior of sputter-deposited Mn-Cr alloys is not examined yet.

Amorphous Cr-Zr alloys are spontaneously passivated showing significantly lower corrosion rates in comparison to the metals in HCl solutions [2]. The synergistic effect of chromium and zirconium in enhancing the corrosion resistance of amorphous Cr-Zr alloys was attributed to the formation of passive double oxy-hydroxide film; which is stable, resistant and more protective compared to the passive films formed on the metals. Accordingly, alloying Mn with both Cr and Zr leads to the formation of a corrosion resistant single phase solid solution. This is a successful way to prepare corrosion-resistant Mn-Zr-Cr alloys that can be used in acidic solutions. It is important to clarify the synergistic effect between Zr and Cr in an alloy matrix containing large amounts of reactive element like Mn.

It is essential to prepare corrosion resistant ferromagnetic manganese (Mn)-based alloys as technologically important alloys for obtaining advanced permanent magnets. In this paper we are aiming at the preparation of corrosion resistant sputter-deposited ternary Mn-Zr-Cr alloys. The effect of alloying manganese with chromium and zirconium on the electrochemical behavior of the prepared ternary alloys in H_2SO_4 solutions represents a main task. For comparison, particular attention was given to the corrosion behavior of sputter-deposited binary Mn-Cr and Mn-Zr alloys, in the same solutions.

2. Experimental

The Mn-Cr, Mn-Zr and Mn-Zr-Cr alloys were prepared on glass substrates by D.C. magnetron sputtering technique. The targets for binary alloys were composed of 99.95% pure chromium or zirconium disks of 100 mm diameter and 5 mm thickness. They were placed on a sputter erosion region consists of 99.9%

pure electro-deposited manganese (ED-Mn) plates of irregular shapes. The target for the preparation of ternary alloys was composed of 99.95% zirconium disk with diameter of 100 mm and 6 mm thickness on which small electro-deposited manganese and chromium disks were placed. The substrates were glass plates of 80 mm in length, 60 mm in width and 1.2 mm in thickness. The glass substrates were cleaned by immersion in water containing a commercial detergent at 75^{o}C. Water cooled three substrates were installed downward in the sputtering chamber facing the target. For the sake of homogenization of the sputter-deposits, the substrates were revolved around the central axis of the chamber, so that the substrates pass right above the target, in addition to the revolution of the substrates themselves around their own axes. After target and substrates were installed the sputtering chamber was evacuated to about 4-9x10^{-7} torr. After pre-sputtering of the target for 30 min, sputtering with argon gas at 4-9x10^{-4} torr was conducted. The composition of the sputter-deposits was controlled by changing the number of small chromium disks and manganese plates on the 100 mm diameter disk, and was determined by electron probe microanalysis (Shimadzu EPMA-C1). The thickness of sputter-deposited alloys were in the range of about 2-3 μm. The structure of the sputter-deposited alloys was identified by X-ray diffraction with Cu Kα radiation at Θ-2Θ mode.

Prior to corrosion, electrochemical and XPS experiments, the samples were mechanically polished with diamond paste up to 0.25 μm to avoid the defects arising from polishing traces. ED-Mn was first abraded with SiC papers up to 2000 grit and then polished with the diamond paste. All tested samples were ultrasonically cleaned in acetone after polishing. The corrosion behavior of the alloys was examined in naturally aerated 1.0 M H_2SO_4 solution at 30^{o}C. The corrosion rates of the binary and ternary alloys were calculated from weight-loss after immersion for different intervals (1 min, and 1, 3 and 168 h) in the acid solution. The size of the samples for the corrosion rate measurements was in the

range 10-15 cm^2. The polarization curves were recorded potentiostatically, and all potentials were measured against and referred to the potential of the SCE (0.245 V vs. the standard hydrogen electrode, SHE). A large area platinum wire was used as a counter electrode. To achieve quasi stationary conditions, a potential sweep rate of 1 mV s^{-1} was used.

X-ray photoelectron spectra were measured by a Shimadzu-ESCA 850 photoelectron spectrometer with Mg Kα excitation for surface analysis. Binding energies were calibrated by the same method described elsewhere [20-22]. The binding energies of Au $3f_{7/2}$ and $3f_{5/2}$ electrons of gold metal and Cu $2p_{3/2}$ and $2p_{1/2}$ electrons of copper metal were taken as 84.07, 87.74, 932.53 and 952.35 eV, respectively, and the kinetic energy of the Cu L_3 $M_{4,5}$ Auger electrons of copper metal were taken as 918.65 eV [21]. The binding energies at the peaks observed in the photoelectron spectra were further corrected by taking the binding energy of C 1 s as 285.5 eV when the specimen showed charging effect [22]. The composition and thickness of the surface films were quantitatively determined by a previously proposed method using integrated intensities of X-ray photoelectron spectra [21-23]. The quantitative determination was performed under the assumption of a three-layer model. Those are an outermost contaminant hydrocarbon layer of uniform thickness, a surface film of uniform thickness and the underlying alloy surface of X-ray photoelectron spectroscopic infinite thickness, along with the assumption of homogeneous distribution of the constituents in each layer. The photo-ionization cross-section of Mn $2p_{3/2}$, Zr 3d and Cr $2p_{3/2}$ electrons relative to that of O 1s electrons used were 2.47 [18] , 2.617 [2] , and 1.71 [2] , respectively.

In order to get information about the in-depth distribution of alloy constituents in the surface film and underlying alloy surface of binary and ternary alloys, angle-resolved measurements were performed, where the angle between the specimen surface and the direction of photoelectron to the detector (take-off angle) was changed by using tilted specimen stages. In such experiments, the surface

sensitivity is varied by changing the angle of detection of the specimen. At low angles of detection with respect to the surface (low take off angle), the signal from the species located in the external part of the film is enhanced whereas at high angles the signal located in the inner part of the film is enhanced [18-24]. Other XPS measurements were carried out at fixed take-off angle of 90°.

3. Results and discussion

Hereafter, all alloy compositions are denoted in atomic percentage and the atomic Cr/ (Cr+Zr) ratio in Mn-Zr-Cr alloys is assigned as N parameter.

3.1. Structure characterization

In general, alloying of zirconium with chromium or manganese via sputter-deposition leads to the formation of binary amorphous Mn-Zr and Cr-Zr alloys in wide composition ranges [2, 14].

Fig. 1 presents XRD diffraction patterns of sputter-deposited Mn-Cr alloys, ED-Mn and sputter-deposited Cr. In this figure, the sputter-deposited alloys containing up to 40at% Cr show typical intense diffraction lines characteristic for crystalline α-Mn phase. Detailed analyses of the XRD patterns of Fig. 1 using Scherrer's equation reveal that the estimated average grain sizes of Mn-Cr alloys are in the range of 15-17 nm [25]. Also, the variation in the lattice spacing of the alloys with the Cr content is not greatly different from that of bcc Cr as shown in Fig. 2. In accordance with the results presented in Fig. 2, it is difficult to confirm the formation of single phase solid solution of nanocrystalline Mn-Cr alloys by recording the continuous change in lattice spacing with the Cr content. No diffraction lines of other precipitated phases in the patterns of the Mn rich Mn-Cr alloys were recorded, therefore it can be said that these alloys consist of single α-Mn phase.

It is well known that the prerequisites for the amorphization of binary alloys by rapid quenching are:

(1) The atomic radius ratio of alloy constituents are smaller than 0.85,

(2) A large negative mixing enthalpy of the constituents, and

(3) The constituents belong to separate groups in the periodic table [26-29].

Alloying Zr with Cr or Mn via sputter-deposition fulfills the prerequisites for amorphization [2,21]. However, alloying Cr with Mn does not fulfill the conditions required for amorphization. The mixing enthalpy of Mn and Cr is far positive (+8.0 kJ mol^{-1}), the atomic radius ratio is 0.99 and both elements belong to the same transition metal group. Fig. 3 shows the composition-structure diagram of sputter-deposited binary and ternary alloy systems i.e. Mn-Cr, Mn-Zr, Cr-Zr and Mn-Zr-Cr. It can be seen that amorphous Mn-Zr-Cr ternary alloys are obtained in a wide composition range in spite of the fact that all Mn-Cr alloys are not amorphized.

3.2. Gravimetric and electrochemical characterization

Fig. 4 presents a comparison of the corrosion rates of sputter-deposited Mn-Zr-Cr alloys, with N value is in the range of 0.28~0.35, in 1.0 M H_2SO_4 solution at 30^{o}C as a function of the Mn content. The corrosion rates of ED-Mn and sputter-deposited Mn-Cr and Mn-Zr binary alloys are also presented for comparison. ED-Mn dissolves instantaneously and the estimated corrosion rate from the weight-loss measurements after immersion in 1.0 M H_2SO_4 solution for 1 h is 4.5 x 10^3 mm y^{-1}. Similarly, sputter-deposited Mn-Cr alloys are dissolved immediately after immersion, and the corrosion rate tends also to decrease with increasing the alloy Cr content. For instance, the Mn-Cr alloy contains 40 at % Cr shows a corrosion rate of more than 100 mm y^{-1}. When Mn is alloyed with Zr, the alloys show lower corrosion rates than those of Mn-Cr alloys, and the corrosion rate tends also to decrease with increasing the alloy Zr content. Therefore, the addition of Zr is more effective in improving the corrosion resistance of Mn in the binary alloy systems. Further improvement in the corrosion resistance is attained when Cr and Zr are

simultaneously added to Mn. The corrosion rates of the Mn-Zr-Cr alloys are about 2-5 orders of magnitude lower than those of the sputter-deposited binary Mn-Zr and Mn-Cr alloys containing relatively the same amount of Mn.

In order to clarify the role of Cr on the corrosion resistance of the ternary amorphous Mn-Zr-Cr system, alloys with different Cr content were prepared and investigated. Fig. 5 shows the change in the corrosion rate of Mn-Zr-Cr alloys containing Mn content in the range of 55-59 at% with N value i.e. Cr/(Cr+Zr) ratio, after immersion in 1.0 M H_2SO_4 solution for one week. The beneficial effect of the simultaneous addition of Cr and Zr compared to the single addition i.e. in binary systems, is clear from this figure. It can be seen that the corrosion rate tends to initially decrease with increasing N value up to 0.66, which corresponds to 58Mn-14Zr-28Cr alloy, then increases again with further increase of N value to 0.75, which corresponds to 59Mn-9.5Zr-30.5Cr alloy. This means that, the increase of Cr content on the expense of Zr content even when the Mn content remains approximately constant, leads to deterioration in the corrosion properties of the ternary alloy.

To confirm the above measurements and to have a good comparison of the corrosion behavior among binary and ternary alloys potentiostatic polarization experiments were carried out. Fig. 6 presents the polarization curves of ternary alloys containing Mn content in the range of 55-59 at% with different N values i.e. Cr/(Cr+Zr) ratios, recorded in 1.0 M H_2SO_4 solution at a scan rate of 1 mV s^{-1} and 30^{o}C. The polarization data were analyzed using the Tafel extrapolation method and the corrosion potential, E_{corr} and the corrosion current density, i_{corr}, were presented in Table 1, which shows that the increase in the N value up to 0.66 decreases i_{corr} and shifts E_{corr} towards noble values. Both E_{corr} and i_{corr} values are adversely affected with further increase of N value to 0.75. The results are in good agreement with those presented in Fig. 6. It is worthwhile to mention that the E_{corr} value for ternary alloys with $N \geq 0.33$ is located in the passivation region of Cr

metal [29] and the corresponding i_{corr} values are in the order of 10^{-4} A m^{-2} (cf. Table 1), indicating the spontaneous passivation of these alloys.

To summarize, the corrosion rates of Mn-Zr alloys are lower than those of Mn-Cr alloys. Nevertheless, the partial substitution of Zr with Cr in the Mn-Zr alloys is effective in decreasing the corrosion rates along with inducing spontaneous passivation. Further, the corrosion rate decreases with increasing the alloy Cr content, if sufficient amount of Zr is present to preserve the desired protection. Accordingly, Cr is effective in enhancing the corrosion resistance in the ternary Mn-Zr-Cr alloys. Also, both Cr and Zr metals act synergistically in improving the corrosion resistance of Mn.

3.3. Surface characterization

In order to understand the previous results and to clarify the role of the alloying elements on the improvement of the corrosion resistance of Mn, XPS analyses for Cr-free and Cr-containing alloys were performed. The presence of C, O, S, Mn, Zr and Cr peaks was identified in the XPS survey spectra of the alloy constituents as demonstrated in Fig. 7. The carbon peak is very small and is originated from contaminant hydrocarbon traces [21,22]. The oxygen contribution (O 1s) was composed of two overlapping peaks corresponding to OM and OH oxygen peaks. The binding energies of these species range between 529.2-529.9 and 531.7-532.2 eV, respectively. The OM oxygen corresponds to O^{-2} ions of the oxide in the surface film. The other oxygen peak initiated from the OH^- ions in the hydration of the surface film [15-22]. The XPS spectra from the alloy constituents indicate the presence of oxidized species coming from the surface and metallic species coming from the underlying alloy surface. The measured spectra of Zr 3d, Mn $2p_{3/2}$ and Cr $2p_{3/2}$ were separated into Zr^{4+} and Zr^m, Mn^{ox} and Mn^m, Cr^{3+} and Cr^m spectra, respectively. The measured spectrum of the Zr 3d consists of two doublet peaks of Zr $3d_{3/2}$ and Zr $3d_{5/2}$ appeared at 177.4 and 180.0 eV corresponding to the metallic Zr^m state and other doublet peaks corresponding to

the Zr^{4+} state recorded at 181.4 and 183.4 eV. The measured spectrum of the Mn $2p_{3/2}$ consists of a peak at 638.4 eV corresponding to metallic state, Mn^{m}, and a major broad peak for the oxidized state. The oxidized peak, Mn^{ox}, consists of three overlapped peaks corresponding to Mn^{2+}, Mn^{3+} and Mn^{4+}. The recorded spectrum of Cr $2p_{3/2}$ consists of two peaks; the low binding energy peak at 573.3 eV was assigned to the metallic state Cr^{m}, the high binding energy peak at 576.5 eV was attributed to Cr^{3+} in the surface film. After integrating intensities of the spectra for individual species, the thickness and composition of the surface film and the composition of the underlying alloy surface were determined quantitatively as reported previously [20,23].

Fig. 8 presents the change in thicknesses of the films formed on the 51Mn-49Zr, 58Mn-28Zr-14Cr and 58Mn-14Zr-28Cr alloys with immersion time in 1.0 M H_2SO_4 solution. The thicknesses of the air-formed films on these alloys are presented for comparison. The thickness of the air-formed films on 51Mn-49Zr, 58Mn-28Zr-14Cr and 58Mn-14Zr-28Cr alloys are 6.0, 5.1 and 4.85 nm, respectively. As can be seen, the thickness of the film formed on the Cr-free Mn-Zr binary alloy increases exponentially with the immersion time, whereas the thickness of films formed on the Mn-Zr-Cr ternary alloys does not increase but tends to slightly decrease with the immersion time. Also, the increase in the alloy Cr content does not affect the film thickness. This indicates the beneficial effect of Cr addition in the formation of a thin, dense and highly protective passive film on the surface of Mn-Zr-Cr ternary alloys in this aggressive acid medium.

Fig. 9 shows the change in the cationic fraction in the surface film and atomic fraction in the underlying surface for chromium-free 51Mn-49Zr alloy as a function of immersion time in 1.0 M H_2SO_4 solution. The composition of the surface film and underlying alloy surface of mechanically polished alloys are presented for comparison. XPS analysis of the alloy surface after mechanical polishing reveals that the air-formed film is enriched with Zr cations, while Mn

metal is resided, mainly, in the underlying alloy surface. This means that the air exposure results in the preferential oxidation of Zr and its enrichment at the surface. The fraction of Zr cations in the surface film increases with immersion time in the electrolyte and the reverse is occurring in the underlying alloy surface. Thus, the apparent increase in the corrosion resistance of Mn by alloying with Zr is due to the high concentration of Zr cations in the surface film.

Figs. 10 and 11 show the change of the cationic fraction in the surface film (a) and atomic fraction in the underlying alloy surface (b) for 58Mn-28Zr-14Cr (N = 0.33) and 58Mn-14Zr-28Cr (N = 0.66) alloys, respectively, with the immersion time in 1.0 M H_2SO_4 solution. The composition of the air-formed film after mechanical polishing and atomic composition beneath this film for the two alloys are also presented for comparison. In both figures, the fractions of Zr and Cr cations in the air-formed film are higher than those in the bulk alloys while Zr and Cr in the underlying alloy surface are slightly deficient. This indicates the preferential oxidation of both metals during air exposure after mechanical polishing. Open circuit immersion in 1.0 M H_2SO_4 solution leads to a rapid initial dissolution of Mn with a significant increase in Cr content in both surface film and underlying alloy surface, while the cationic and atomic fractions of Zr remain constant. It is also worth noticed that the composition of the passive films formed on the 58Mn-28Zr-14Cr and 58Mn-14Zr-28Cr alloys attain their steady state after 250 and 65 min of electrode immersion in the acid solution, respectively. The cationic fractions of Mn in the passive films of 58Mn-28Zr-14Cr and 58Mn-14Zr-28Cr alloys are 0.25 and 0.16 and its atomic fractions in the underlying alloy surfaces are 0.62 and 0.46, respectively. Hence, the decrease in Mn content along with an increase in Cr content in both the surface film and underlying alloy surface is required to maintain fast spontaneous passivation and enhance the corrosion resistance in the H_2SO_4 solution. Similar trend was observed for sputter-deposited Mn-Ta-Cr alloys after their open circuit immersion 1.0 M H_2SO_4 solution [15] and

for Al-Cr-Mo alloys during potentiostatic polarization in 1.0 M HCl solution [24]. It is also worth mentioning that Cr has a well-known high activity for cathodic proton reduction in acidic medium [2, 21]. It seems that the increase in alloy Cr content decreases the corrosion rate via an increase in the cathodic current density which leads to fast initial dissolution of Mn unnecessary for passivation with a subsequent enrichment of Cr on both surface film and underlying alloy surface.

In order to get additional information about the beneficial role of Cr and to characterize in-depth distribution of the alloy components in the surface film as well as in the underlying alloy surface, angle-resolved XPS analysis was performed. Fig. 12 shows changes in the ratios of $[O^{-2}]$/[Cation] and $[OH^{-}]$/[Cation] in the surface films for Cr-free 51Mn-49Zr and 58Mn-14Zr-28Cr alloys after immersion in 1.0 M H_2SO_4 solution for 30 min as a function of photoelectron take-off angle. From this figure, the surface film of both binary and ternary alloys is composed of oxy-hydroxide, where the interior part is rather dry and well developed by M-O-M Bridge, while the exterior part is wet with OH^{-} ions. The surface film of Cr-free 58Mn-49Zr alloy shows higher ratios of O^{2-} and OH^{-} ions throughout the film than those in the passive films formed on the ternary alloys. Furthermore, the ratios of $[O^{-2}]$/[Cation] and $[OH^{-}]$/[Cation] in the film formed on Cr-free 51Mn-49Zr alloy is quite dependent on the take-angle of the photoelectrons, whereas the ratio of $[O^{-2}]$/[Cation] and $[OH^{-}]$/[Cation] in the film formed on spontaneously passivated ternary alloys changes slowly with the change in the take-angle. This result supports the fact that the oxy-hydroxide passive films formed on the ternary alloys on immersion in 1.0 M H_2SO_4 solution are thin, dense and compact compared to the thick porous film formed on Cr-free 51Mn-49Zr alloy. Fig. 13 shows the changes in cationic fraction in the surface film and atomic fraction in the underlying alloy surface of Cr-free 51Mn-49Zr alloy after immersion in 1.0 M H_2SO_4 solution for 30 min as a function of take-off angle of the photoelectrons. The depth profiling of Mn-Zr alloy shows a clear concentration

gradient with majority of Zr cations and metallic Mn in the exterior parts of both surface film and underlying alloy surface, respectively.

Figs. 14 shows the changes in cationic fraction in the surface film (a) and atomic fraction in the underlying alloy surface (b) for spontaneously passivated 58Mn-14Zr-28Cr (N = 0.66) alloys after immersion in 1.0 M H_2SO_4 solution for 30 min as a function of the take-off angle of the photoelectrons. In this figure, the depth profiling reveals that the exterior parts of passive film and underlying alloy surface are obviously enriched with Cr, whereas Zr and Mn are concentrated in the interior parts.

Fig. 15 presents the binding energies of Cr^{3+} $3P_{3/2}$ (a) and Zr^{4+} $3d_{5/2}$ (b) electrons as a function of the cationic fractions of Cr in the surface film of binary and ternary alloys after immersion in 1.0 M H_2SO_4 solution. The peaks of the binding energy gradually change with the Cr fraction in the surface film in a similar manner to that observed for binary Cr–Zr alloys in concentrated hydrochloric acid solution [2]. In Fig. 15(a), the binding energy peak of Cr^{3+} $3P_{3/2}$ electrons increases with increasing the fractions of Zr cations in the film, while in Fig. 15(b) the binding energy peak of Zr^{4+} $3d_{5/2}$ electrons decreases with increasing the fraction of Cr cations in the passive film. This indicates the occurrence of charge transfer from Cr^{3+} to Zr^{4+} ions and confirms that Cr and Zr cations are located in close proximity in the passive film so as to show such an electronic interaction. In other words, passivating Cr^{3+} and Zr^{4+} cations do not exist in separate form in the surface film but in the form of a mixed oxy-hydroxide, which is responsible for the high corrosion resistance of the ternary Mn-Zr-Cr alloys.

4. Conclusion

Binary Mn-Zr and Mn-Cr, and ternary Mn-Zr-Cr alloys were prepared by sputter-deposition method in a wide composition range and their corrosion behavior was examined in 1.0 M H_2SO_4 solution. The corrosion rates of Mn-Zr

binary alloys are lower than those of the Mn-Cr alloys. The partial substitution of Zr with Cr in the Mn-Zr alloys is effective in decreasing the corrosion rates along with inducing spontaneous passivation in the presence of sufficient amounts of Zr. According to XPS analysis, the spontaneously passivated films on the ternary Mn-Zr-Cr alloys are composed of mixed oxy-hydroxide of Cr and Zr cations. This mixed oxy-hydroxide film is responsible for the high corrosion resistance of the alloys, which increases with increasing Cr concentration in both passive film and the underlying alloy. The Cr enrichment in the underlying alloy surface occurs in the exterior part of the outermost metallic layer at the alloy/passive film interface. This stabilizes the alloy/film interface leading to further improvement in the protective nature of the oxy-hydroxide passive film.

Acknowledgements

The sputter-deposited alloys were prepared by Dr. A.A. El-Moneim in the Institute of Materials Research (IMR), Tohoku University, Sendai, Japan. The authors are grateful for the facilities provided by Professor K. Hashimoto for the characterization of the prepared materials.

References

[1] J.H. Kim, E. Akiyama, H. Yoshioka, H . Habazaki, A. Kawashima, K. Asami, K. Hashimoto, The corrosion behavior of sputter-deposited amorphous titanium-chromium alloys in 1 M and 6 M HCl solutions, Corros. Sci. 34 (1993) 975-988.

[2] J. H. Kim, E. Akiyama, H. Habazaki, A. Kawashima, K. Asami and K. Hashimoto, The corrosion behavior of sputter-deposited amorphous chromium-zirconium alloys in 6 M HCl solution, Corros. Sci., 34 (1993) 1817–1827.

[3] J. H. Kim, Akiyama, H. Habazaki, A. Kawashima, K. Asami, K. Hashimoto, An XPS study of the corrosion behavior of sputter-deposited amorphous Cr-Nb and Cr-Ta alloys in 12 M HCl solution, Corros. Sci. 34 (1994) 511-523.

[4] P.Y. Park, E. Akiyama, H. Habazaki, A. Kawashima, K. Asami , K. Hashimoto, The corrosion behavior of sputter-deposited amorphous Mo-Zr alloys in 12 M HCl, Corros. Sci. 37 (1995) 307-320.

[5] J. Bhattarai, E. Akiyama, H. Habazaki, A. Kawashima, K. Asami and K. Hashimoto, Electrochemical and XPS studies of the corrosion behavior of sputter-deposited W-Nb alloys in concentrated hydrochloric acid solutions, Corros. Sci. 40 (1998) 19-42.

[6] A.A. El-Moneim, E. Akiyama, K.M. Ismail, K. Hashimoto, Corrosion behavior of sputter-deposited Mg–Zr alloys in a borate buffer solution, Corrosion Science, Corros. Sci. 53 (2011) 2988-2993.

[7] K. Hashimoto, N. Kumagai, H. Yoshioka, J.H. Kim, E. Akiyama, H. Habazaki, S. Mrowec, A. Kawashima, K. Asami, Corrosion-resistant amorphous surface alloys, Corros. Sci. 35 (1993) 363–370.

[8] K. Hashimoto, P. Y. Park, J. H. Kim, E. Akiyama, H. Habazaki, A. Kawashima, K. Asami, Similarity and difference in roles of chromium and molybdenum in passivating amorphous alloys in concentrated acids, Mater. Sci. Forum, 185 (1995) 779-781.

[9] P.Y. Park, E. Akiyama, H. Habazaki, A. Kawashima, K. Asami, K. Hashimoto, The corrosion behavior of sputter-deposited Mo-Ti alloys in concentrated hydrochloric acid, Corros. Sci. 38 (1996) 1649–1667.

[10] P.Y. Park, E. Akiyama, H. Habazaki, A. Kawashima, K. Asami, K. Hashimoto, The corrosion behavior of sputter-deposited Mo-Nb alloys in 12 M HCl solution, Corros. Sci. 38 (1996) 1731–1750

[11] P.Y. Park, E. Akiyama, A. Kawashima, K. Asami, K. Hashimoto, The corrosion behavior of sputter-deposited Mo-Ta alloys in 12 M HCl solution, Corros. Sci. 38 (1996) 397–411.

[12] A.A. El-Moneim, B.P. Zhang, E. Akiyama, H. Habazaki, A. Kawashima, K. Asami, K. Hashimoto, The corrosion behaviour of sputter-deposited amorphous Mn-Ti alloys in 0.5 M NaCl solutions, Corros. Sci. 39 (1997) 305–320.

[13] A.A. El-Moneim, E. Akiyama, H. Habazaki, A. Kawashima, K. Asami, K.Hashimoto, The corrosion behaviour of sputter-deposited amorphous Mn-Ta alloys in 0.5 M NaCl solution, Corros. Sci. 39 (1997) 1965–1979.

[14] A.A. El-Moneim, E. Akiyama, H. Habazaki, A. Kawashima, K. Asami, K. Hashimoto, Passivity and its breakdown on sputter-deposited amorphous Mn-Zr alloys in neutral chloride solutions, Corros. Sci. 40 (1998) 235–250.

[15] A.A. El-Moneim, E. Akiyama, H. Habazaki, A. Kawashima, K. Asami, K. Hashimoto, The effect of alloying elements on the corrosion behaviour of sputter-deposited amorphous Mn–Ta–Cr alloys in 1 M H_2SO_4, Corros. Sci. 40 (1998) 1491–1512.

[16] A.A. El-Moneim, E. Akiyama, H. Habazaki, A. Kawashima, K. Asami, K. Hashimoto, XPS and electrochemical studies on the corrosion behavior of Mn-Nb alloys in neutral chloride-containing solution, Corros. Sci. 40 (1998) 1513–1531.

[17] K.M. Ismail, A.A. El-Moneim, W.A. Badawy, Stability of sputter-deposited amorphous Mn-Ta Alloys in chloride-free and chloride-containing H_2SO_4 solution, J. Electrochem. Soc. 148 (2001) C81–C87.

[18] A.A. El-Moneim, K.M. Ismail, W.A. Badawy, Electrochemical and XPS studies of sputter-deposited ternary Mn–Ta–Cr alloys in chloride-free and chloride-containing, Electrochim. Acta 47 (2002) 2463–2472.

[19] A. A. El-Moneim, M. Bakr Mahmoud, New composite anodes for oxygen evolution during seawater electrolysis, Inter. J. Electrochem. Sci. 7 (2012) 671–685.

[20] K. Asami, A precisely consistent energy calibration method for X-ray photoelectron spectroscopy, J. Electron Spectroscopy 9 (1976) 469–478.

[21] A.A. El-Moneim, H. Habazaki, A. Kawashima, K. Asami, K. Hashimoto, Corrosion-resistant Mn-Zr-Cr alloys in chloride-containing media, Materials Science and Engineering A 267 (1999) 285-293.

[22] A.A. El-Moneim, K.M. Ismail, W.A. Badawy, Sputter-Deposited Mg-Zr Alloys- Surface Characteristics and Electrochemical behavior in Borate Solutions, Zeitschrift für Physikalische Chemie. 228(9) (2014) 901–916.

[23] K. Asami, K. Hashimoto, The X-ray photo-electron spectra of several oxides of iron and chromium, Corros. Sci. 17 (1977) 559–570.

[24] E. Akiyama, H. Habazaki, A. Kawashima, K. Asami, K. Hashimoto, An angle-resolved xps study of the in-depth structure of passivated amorphous aluminum alloys, Corros Sci. 39 (1997) 1351-1364.

[25] P. Scherrer, Nachr. Ges. Wiss. Gottingen 26 (1918) 98–100.

[26] B. C. Giessen, in Proc 4th Int. Conf. on Rapidly Quenched Metals, Vol. 1 ed T. Masumoto and K. Suzuki, Japan Institute of Metals, Sendai, 1981, p. 213.

[27] I.J. Polmear, Recent trend in light metal alloys, J. Mater.Trans, JIM. 37 (1996) 12.

[28] I. Egami and Y. Waseda, Binary metallic glass alloy systems, J. Non –Cryst. Solids. 64 (1984) 113-134.

[29] M. Li and W.L. Johnson, Instability of metastable solid solutions and the crystal to glass transition, Phys. Rev. Lett. 70 (1993) 1120-1123.

Figure captions

Fig. 1: XRD patterns for ED-Mn and sputter deposited Cr and Mn-Cr alloys.

Fig. 2: Lattice spacing of sputter-deposited Mn-Cr alloys plotted as function of Cr content.

Fig. 3: The composition-structure diagram of sputter-deposited binary and ternary alloy systems.

Fig. 4: Corrosion rates of sputter-deposited Mn-Cr, Mn-Zr and Mn-Zr-Cr alloys plotted as a function of Mn content. Corrosion rate of ED-Mn metal is shown for comparison.

Fig. 5: Change in the corrosion rate of sputter-deposited amorphous 55-59Mn-Zr-Cr alloys as a function of Cr/ (Cr+Zr) ratio.

Fig. 6: Potentiostatic polarization curves of sputter-deposited amorphous 55-59Mn-Zr-Cr alloys having different N = Cr/(Cr+Zr) ratios. Potentiodynamic polarization curves of sputter-deposited Mn-Zr alloy is also shown for comparison. Scan rate 1 mV s^{-1} at 30^{o}C.

Fig. 7: Diagrammatic sketch of XPS analyses of a three layers model used for estimating the thickness and composition of surface films and underlying alloy surface.

Fig. 8: Thickness of the surface film formed on Mn-49Zr and 58Mn-14Zr-28Cr and 58Mn-28Zr-14Cr alloys plotted as a function of immersion time in 1 M H_2SO_4 solution at 30^{o}C.

Fig. 9: Cationic fractions in the surface film and atomic fractions in the underlying alloy surface for 51Mn-49Zr alloy, plotted as a function of immersion time in 1 M H_2SO_4 solution at 30^{o}C.

Fig. 10: Cationic fractions in the passive film (a) and atomic fractions in the underlying alloy surface (b) formed on 58Mn-28Zr-14Cr alloy (N = 0.33) plotted as a function of immersion time in 1 M H_2SO_4 solution at 30^oC.

Fig. 11: Cationic fractions in the passive film (a) and atomic fractions in the underlying alloy surface (b) formed on 58Mn-14Zr-28Cr (N= 0.66) plotted as a function of immersion time in 1 M H_2SO_4 solution at 30^oC.

Fig. 12: Ratios of [O^{-2}]/[Cation] and [OH^-]/[Cation] in the surface films formed on 51Mn-49Zr and Mn-28Zr-14Cr alloys plotted as a function of photoelectron take-off angle after immersion in 1 M H_2SO_4 solution for 30 min at 30^oC.

Fig. 13: Cationic fractions in the surface film and atomic fractions in the underlying alloy surface for 51Mn-49Zr alloy plotted as a function of photoelectron take-off angle after immersion in 1 M H_2SO_4 solution for 30 min.

Fig. 14: Cationic fractions in the surface film (a) and atomic fractions in the underlying alloy surface (b) for Mn-14Zr-28Cr alloy (N = 0.66) plotted as a function of photoelectron take-off angle after immersion in 1 M H_2SO_4 solution for 30 min at 30^oC.

Fig. 15: The Binding Energies of Zr^{4+} (a) and Cr^{3+} (b) electrons plotted as a function of cationic fractions of chromium in the surface film formed on Mn-Zr-Cr alloys after immersion 1 M H_2SO_4 solution at 30^oC.

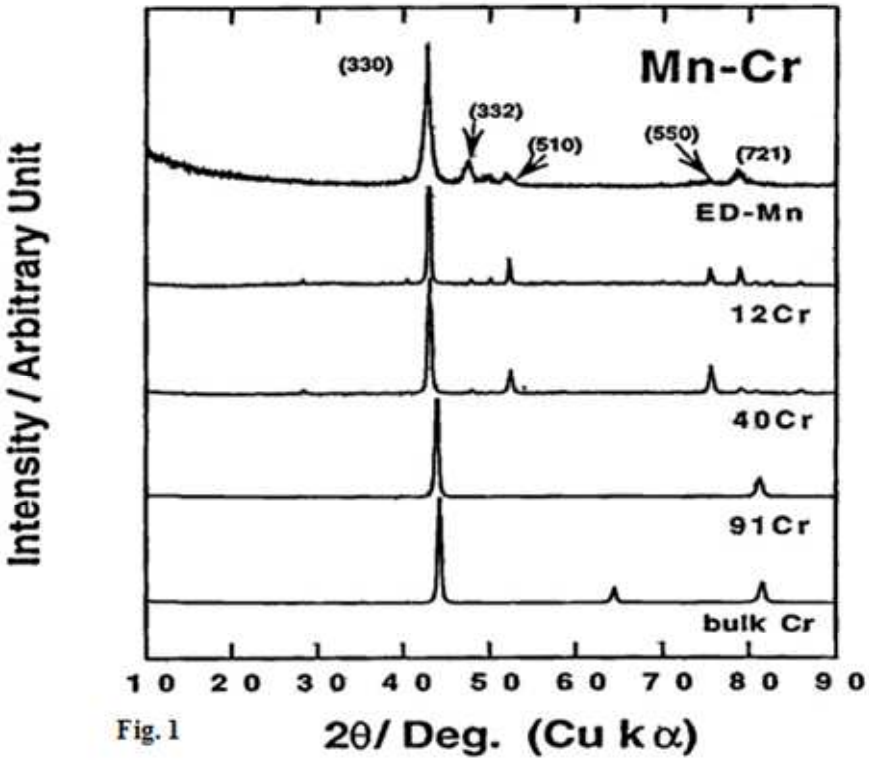

Fig. 1

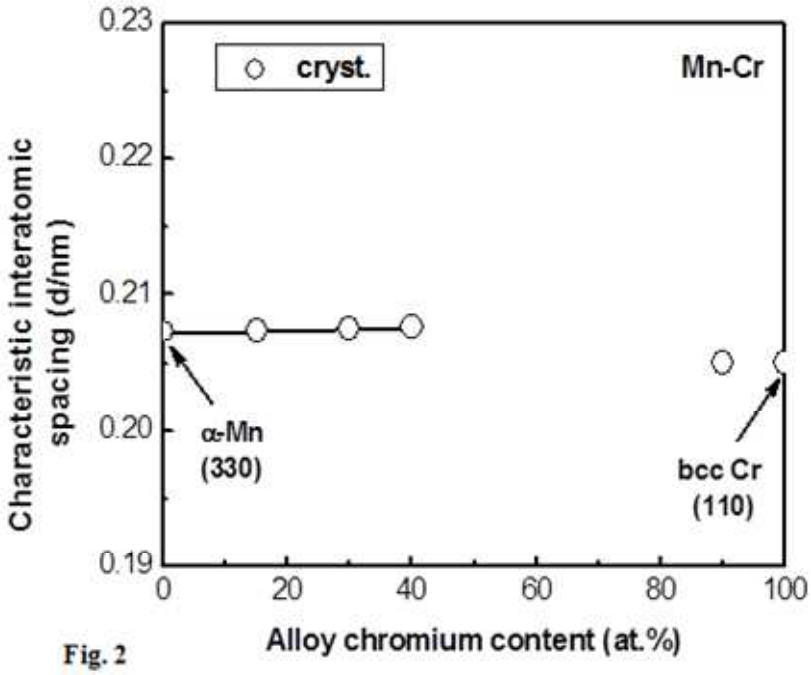

Fig. 2

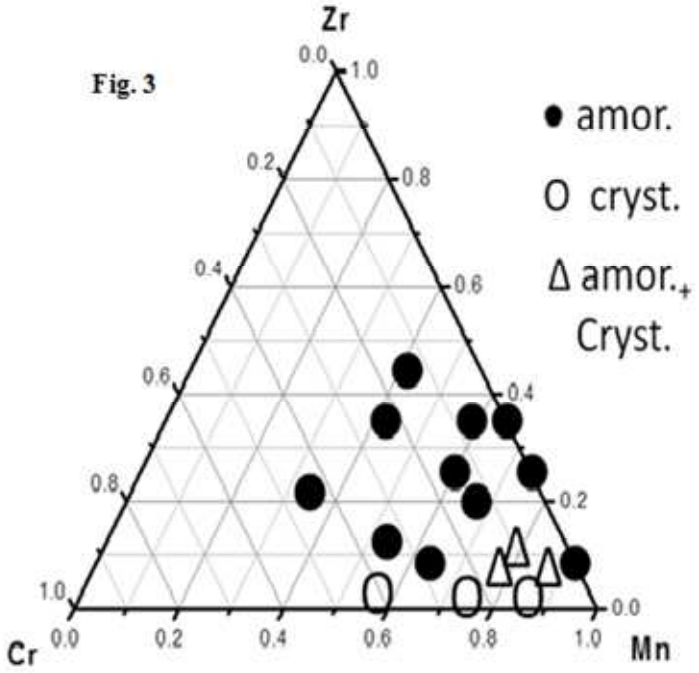

Fig. 3

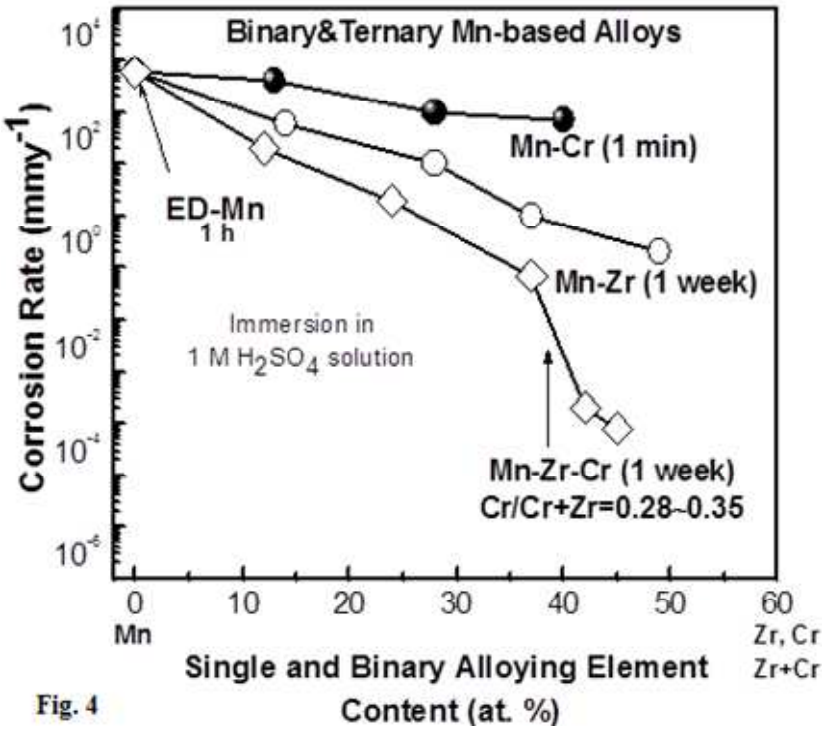

Fig. 4

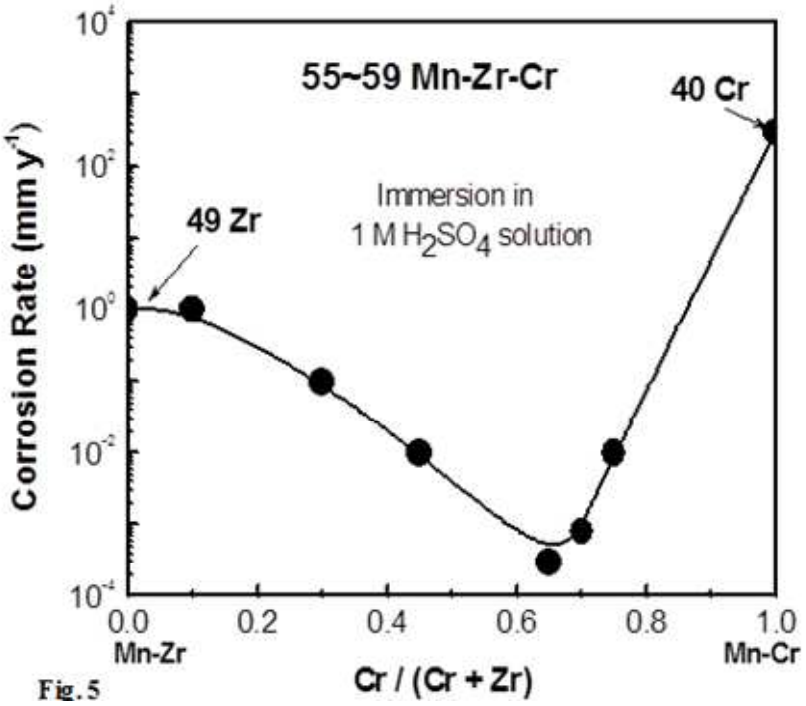

Fig. 5

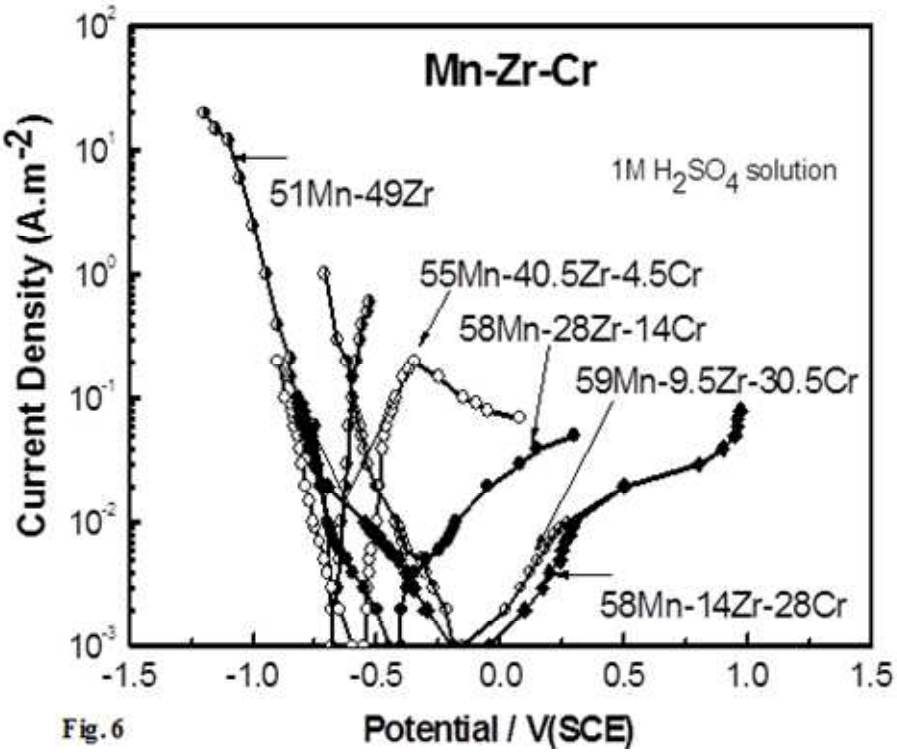

Fig. 6

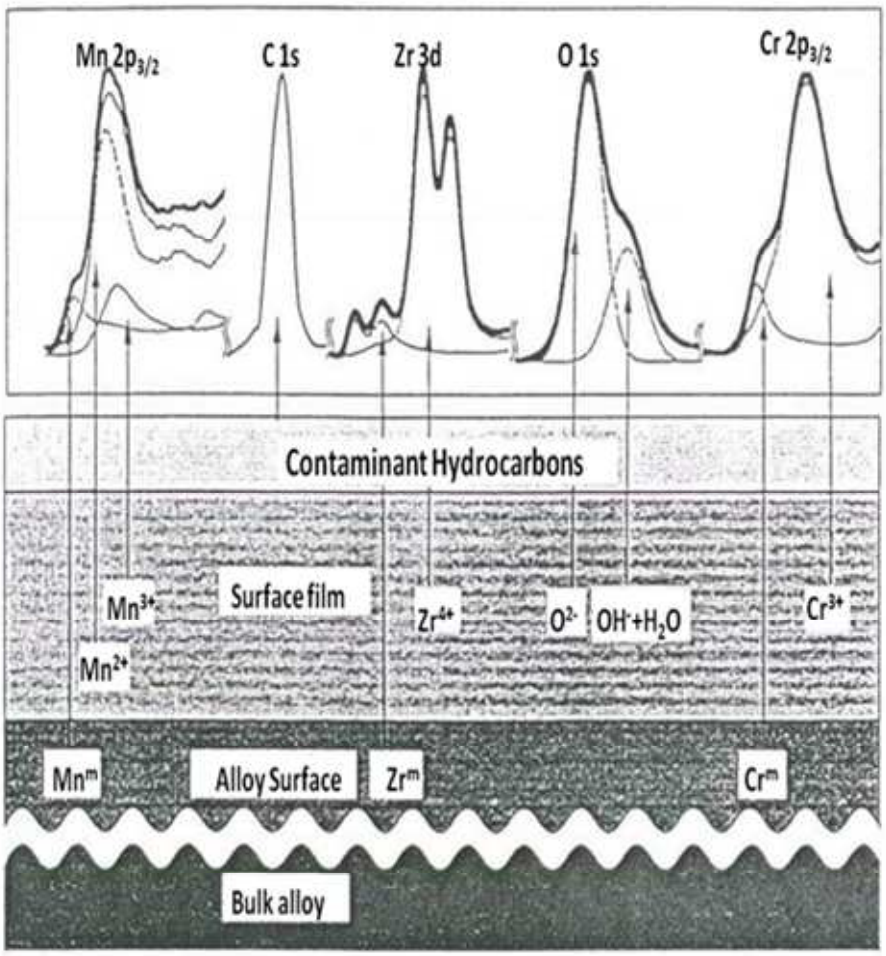

Fig. 7

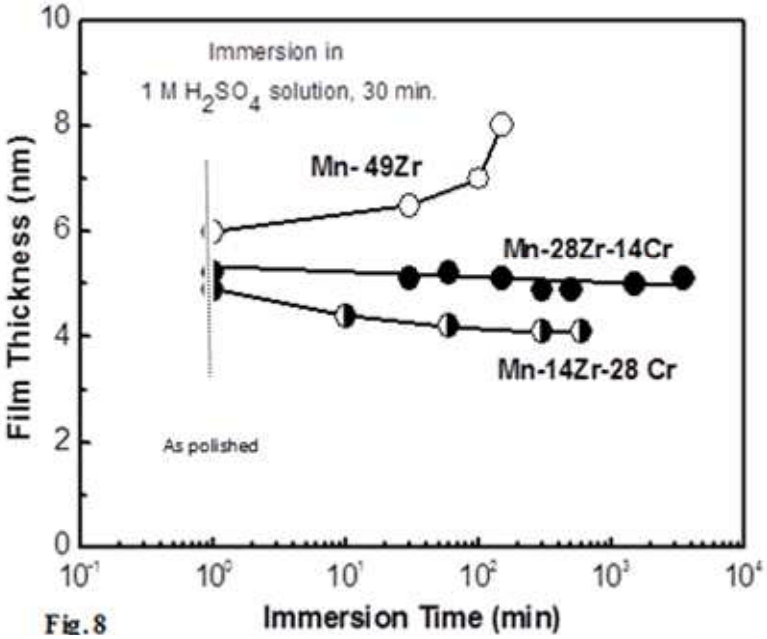

Fig. 8

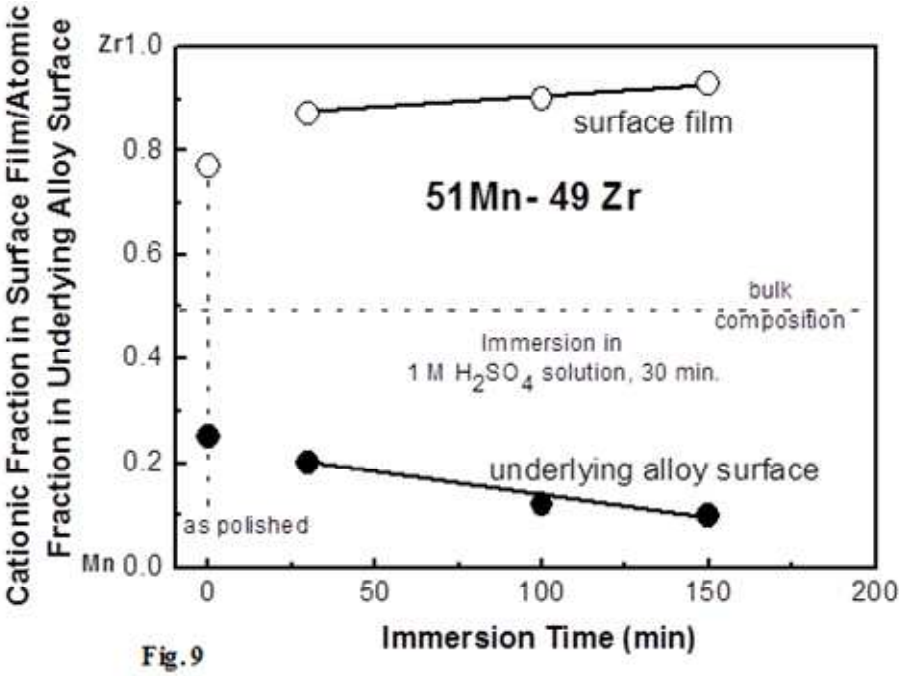

Fig.9

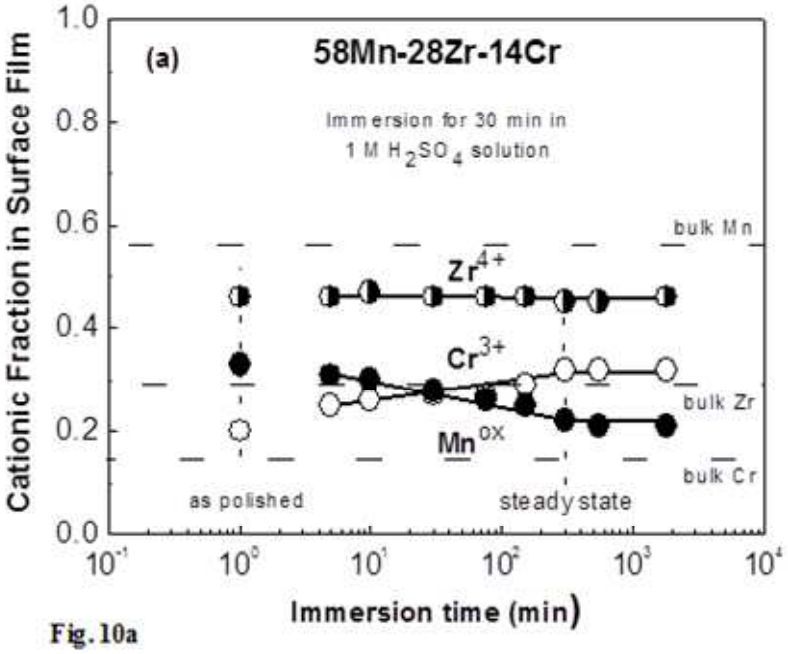

Fig.10a

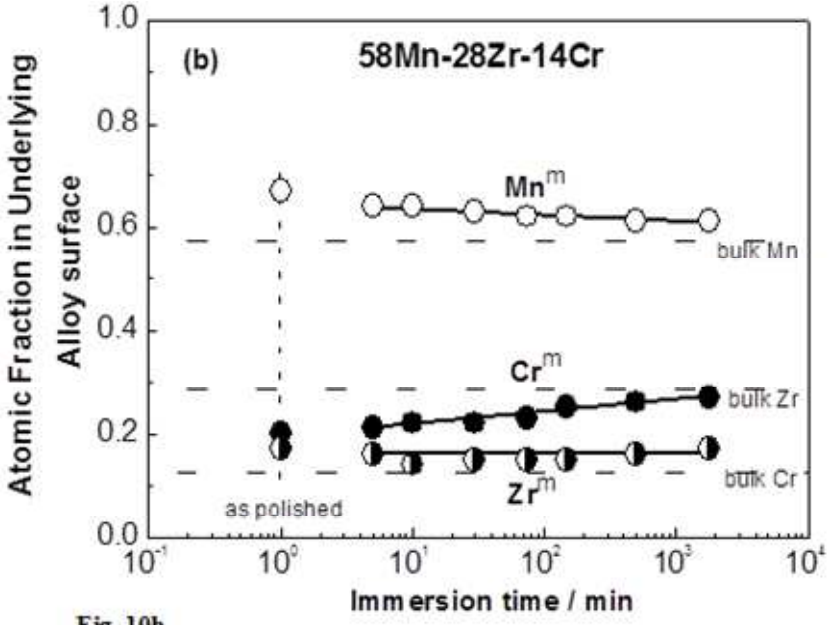

Fig. 10b

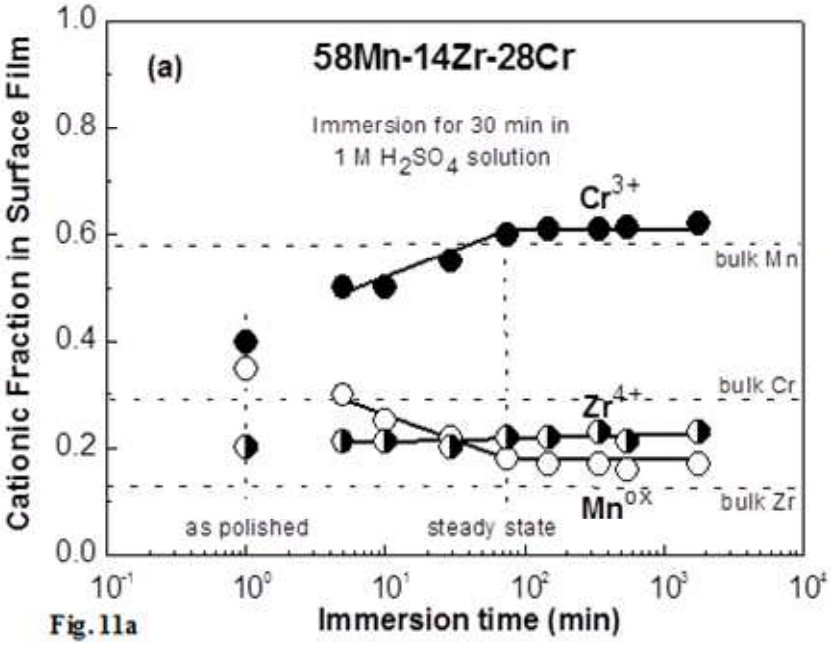

Fig. 11a

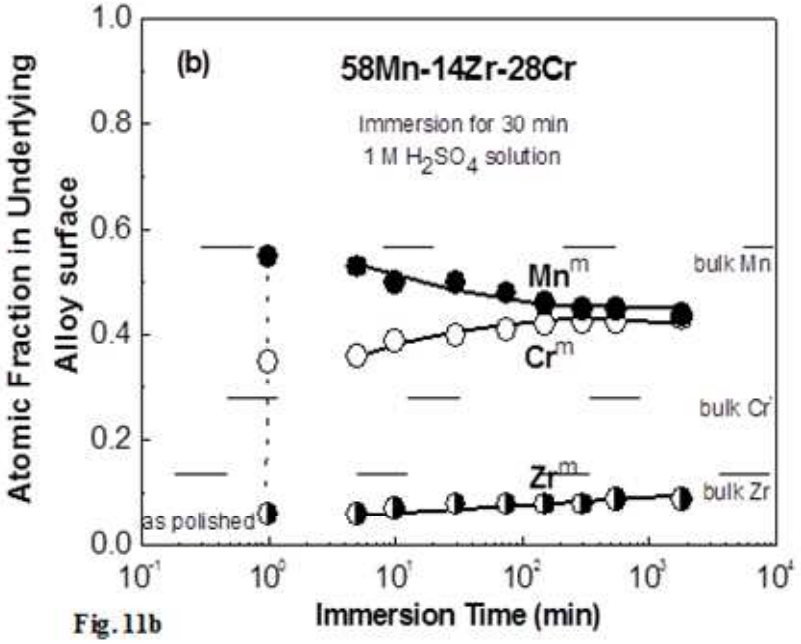

Fig. 11b

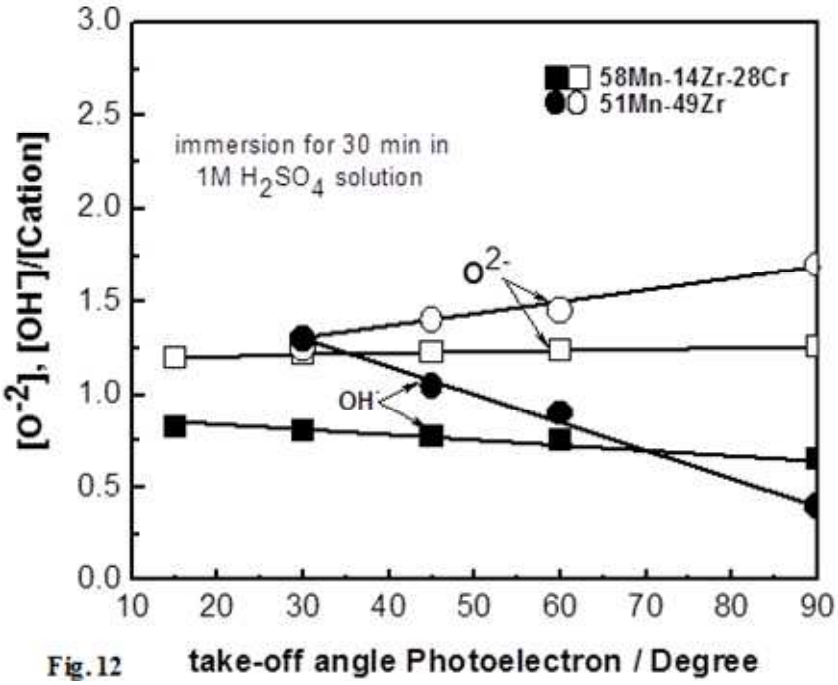

Fig. 12

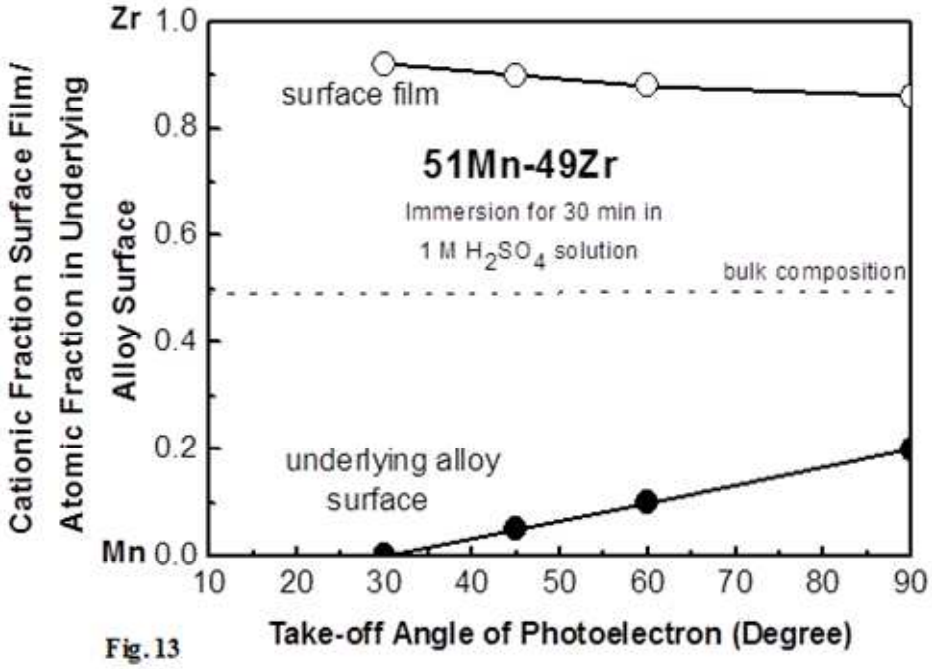

Fig. 13

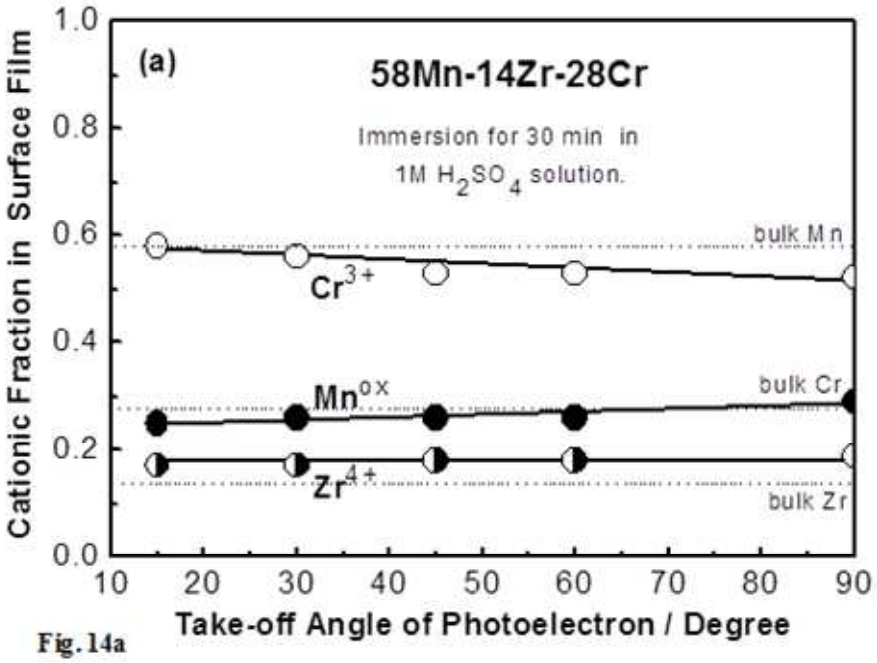

Fig. 14a

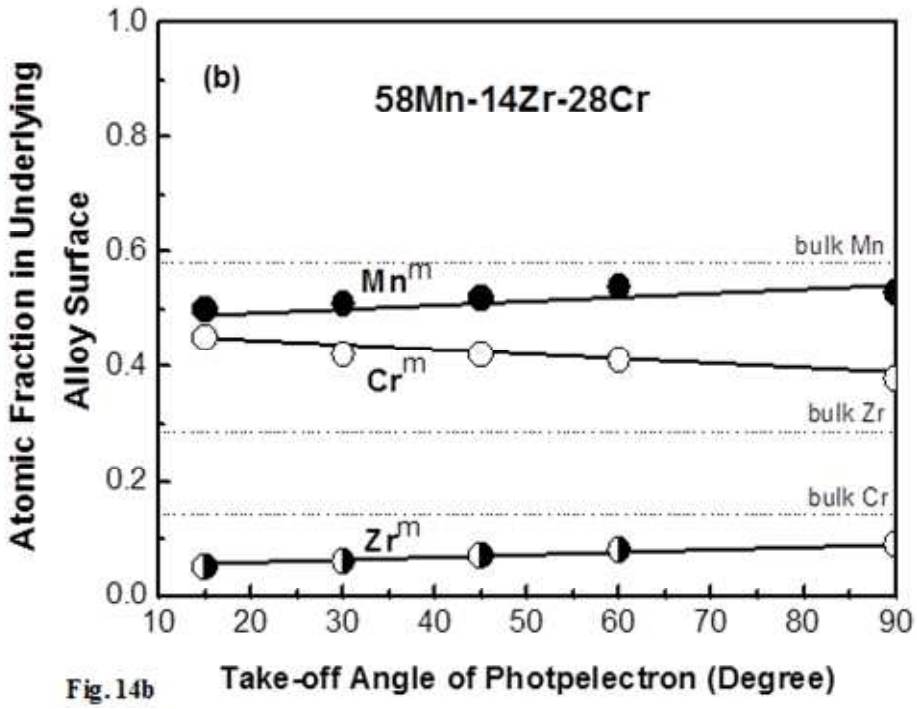

Fig. 14b

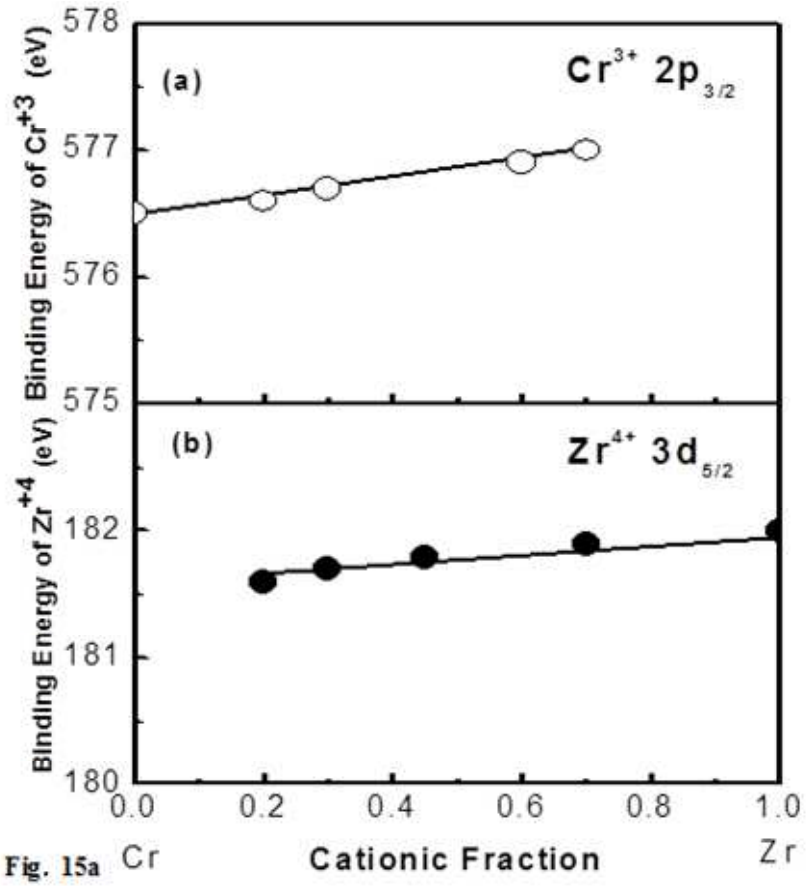

Fig. 15a

Table 1

The corrosion potential, E_{corr} and corrosion current density, i_{corr}, for the different sputter-deposited amorphous alloys obtained after potentiodynamic polarization in 1 M H_2SO_4 at a scan rate of 1 mV s^{-1} and 30°C.

Alloy (N = Cr/(Cr+Zr))	$E_{corr.}$, V (SCE)	$i_{corr.}$ (μA cm^{-2})
Amorph. / Mn-49Zr (N =0.0)	-0.670	19.0
Amorph./55Mn-40.5Zr-4.5Cr (N=0.1)	-0.580	1.90
Amorph./58Mn-28Zr-14Cr (N=0.33)	-0.490	0.03
Amorph./58Mn-14Zr-28Cr (N=0.66)	-0.120	0.10
Amorph./59Mn-9.5Zr-30.5Cr (N=0.75)	-0.170	0.20